PRELIMINARY SPECTRAL ANALYSIS OF THE RAM ACCELERATOR

by
Amy E. Prochko

A thesis submitted in partial fulfillment
of the requirements for the degree of

Master of Science
in
Aeronautics and Astronautics

University of Washington
1991

Approved by _____
(Chairperson of the Supervisory Committee)

Program Authorized
to Offer Degree Department of Aeronautics and Astronautics

Date _____

In presenting this thesis in partial fulfillment of the requirements for a Master's degree at the University of Washington, I agree that the Library shall make its copies freely available for inspection. I further agree that extensive copying of this thesis is allowable only for scholarly purposes, consistent with "fair-use" as prescribed in the U.S. Copyright Law. Any other reproductionfor any purposes or by any means shall not be allowed without my written permission.

Signature _____

Date _____

University of Washington
Abstract

Preliminary Spectral Analysis of the Ram Accelerator

by Amy E. Prochko

Chairperson of the Supervisory Committee:
Professor Adam P. Bruckner
Department of Aeronautics and Astronautics

Preliminary experiments to acquire spectral diagnostics were planned and implemented to investigate the acceleration of projectiles to ultrahigh velocities using an in-tube ramjet concept called the ram accelerator. A projectile is fired into a tube filled with a premixed high-pressure gaseous propellant. The projectile resembles the centerbody of a conventional ramjet. The combustion process travels with the projectile generating a pressure distribution which produces forward thrust on the projectile. When the heat release of combustion is too high, the combustion process sweeps over the front of the projectile and travels at the Chapman-Jouguet (C-J) detonation velocity of the mixture. This phenomenon is called an unstart. Time-integrated visible and near infrared spectral data were acquired during operation in a propellant gas comprised of methane, oxygen and helium. Concurrent measurements of velocity, pressure and luminosity were obtained relative to the spectrometer station in the tube for most of the shots. The premixed gas pressures in the section where the spectrometer was located ranged from 31 to 43 atm. In normal operation, the velocity of the vehicle as it passed the spectrometer ranged from 2270 to 2380 m/s. Spectral data collected in the near infrared revealed absorption lines. Otherwise, continuum emission, presumably from carbon particles, was generally displayed.

Table of Contents

List of Figures

List of Tables

ACKNOWLEDGEMENTS

I would like to express my appreciation to my adviser Professor Adam P. Bruckner, and to Professor Abraham Hertzberg and Professor Scott Winter for their support.

Many thanks are deserved by my fellow graduate students working on the ram accelerator project. These people are Carl Knowlen, Gilbert Chew, Jackie Auzias de Turenne, Barbrina Dunmire (my dependable snow-weather friend), Robert Macintosh, John Hinkey, Mrs. Jian-Guo Li, Matt Jardin, and especially, Edward Burnham, whose help and encouragement were invaluable. Yes, where there is a will, there is a way!

A bolshoyuh spaseeba (big thanks) is due to Nick Loebel of the Bioengineering department without whose advise and optical equipment I would have been at a loss. Thanks also go to Alan Kull for his encouragement and consultation. Most of all, I am indebted to Patrick Wadell of the Astronomy department without whose expertise and equipment I would not have had the luxury to acquire this data.

DEDICATION

To Mom and Dad, whose love and support have made me strong.

Chapter 1

Introduction

The ram accelerator is a ramjet in-tube concept for accelerating projectiles to very high velocities. The propulsion process is similar to that of a conventional air breathing ramjet. The projectile resembles the centerbody of a ramjet, but carries no on-board propellant. It is launched into a tube of premixed, high-pressure gaseous fuel and oxidizer. After ignition, the heat release of combustion sustains a pressure distribution on the projectile body producing forward thrust. The pressure, chemical composition, energy density and speed of sound are chosen to optimize thrust over the desired velocity range. To maintain high thrust and efficiency over a broad velocity regime, the projectile flies through several separate mixtures each having a higher acoustic speed than the preceeding one. Several modes of ram accelerator operation which span the velocity range of 0.7 to 12 km/sec have been proposed.[1] These include a thermally choked subsonic combustion mode, shown in Fig.1.1, and two superdetonative modes.[1-6] The thermally choked subsonic mode has been extensively studied at the University of Washington[1-5] reaching velocities in excess of 2600 m/sec.

The steady state operation of the thermally choked subsonic mode can be compared to the operation of a ramjet. In a ramjet, the supersonic flow enters the diffuser where it is compressed by a system of oblique shocks (Fig. 1.2). The flow, which is still supersonic, passes through the throat of the diffuser and expands. The flow is then rendered subsonic by a normal shock. The position of the normal shock is controlled by a combination of subsonic heat addition and area contraction of the exit nozzle. The relation between the heat addition and area contraction is that the flow chokes. In the ram accelerator, the tube represents the outer cowling of the ramjet. Since there is no area contraction, the heat release of the mixture controls the position of the normal shock. When the heat release is not great enough to support the wave on the projectile, the normal shock moves backward, off the projectile, and thrust goes to zero. When the heat release is too great, the combustion sweeps forward over the nose of the projectile, usually resulting in an upstream propagating detonation wave. Ram accelerator propulsion is only achieved when

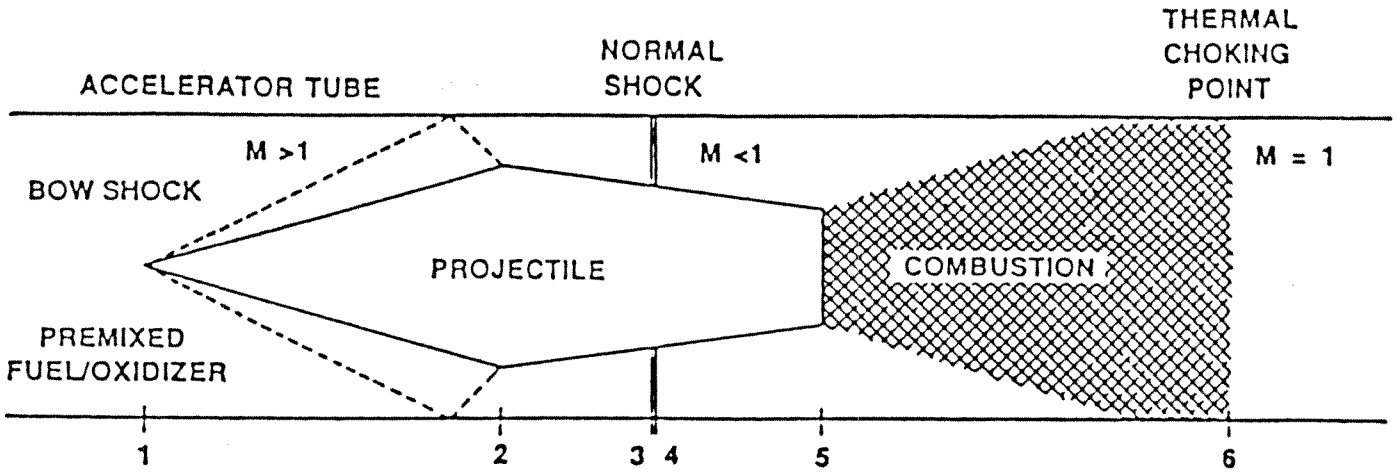

Fig. 1.1: Thermally choked subsonic combustion mode.

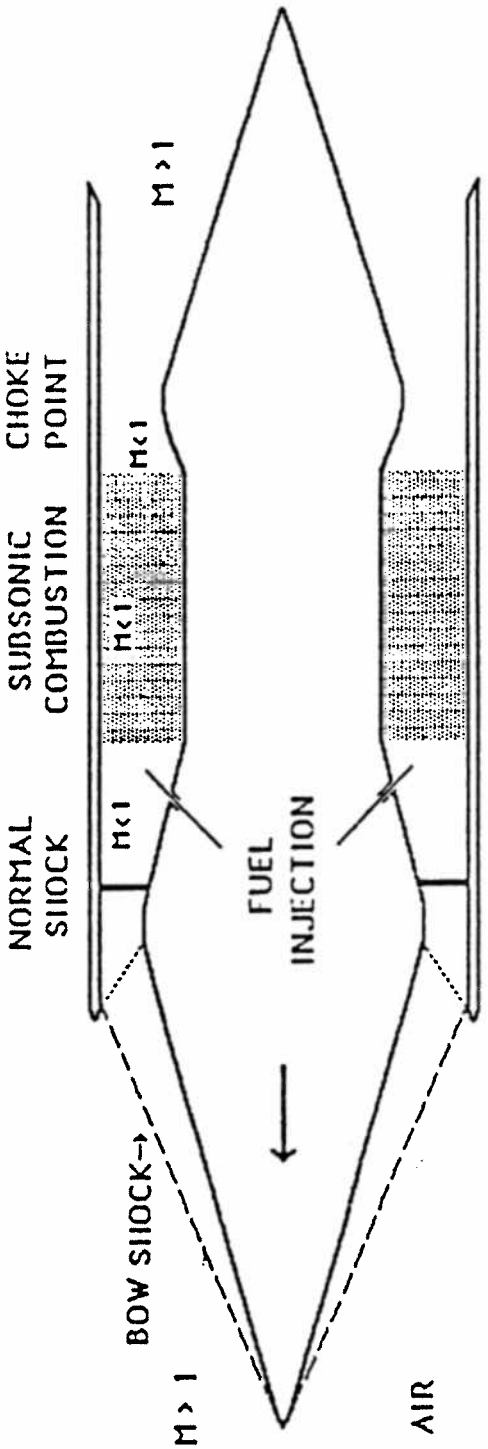

Fig. 1.2: Ramjet configuration.

the normal shock stays on the projectile behind the throat. Whenever the combustion sweeps forward of the throat, it is called an unstart.

The performance of the thermally choked ram accelerator mode is currently described by a one-dimensional quasi-steady-state model employing equilibrium combustion chemistry.[2] This model accurately estimates the thrust on the projectile from steady-state values of the flow, but does not take into effect the unsteady, turbulent behavior of the combustion products. An unsteady model of the ram accelerator has been developed[7], but a true model of the heat release has yet to be formulated. A computer model has also been developed for general combustion kinetics[8], but has not been integrated into an unsteady numerical code. To fully model ram accelerator operation, an unsteady code complete with finite rate chemistry is needed. In order to properly model the heat release, experimental data are needed. Spectral features as a function of time would be ideal. This thesis is a first step in the direction of providing insights for a model of the heat release.

Chapter 2 presents the ram accelerator facility and instrumentation as well as the model of the combustion zone. The data analysis and experimental apparatus used to obtain the spectral data are described in Chapter 3. Time-integrated spectroscopic data from both the thermally choked subsonic combustion mode and the unstart mode are presented in Chapter 4. Finally, conclusions and steps to obtain the information needed for modeling the heat release of the ram accelerator are outlined.

Chapter 2

Background

The ram accelerator facility and instrumentation are described in this chapter. In addition, a model of the combustion zone is presented.

2.1 Ram Accelerator Facility

The ram accelerator facility (Fig. 2.1) consists of a light gas gun, ram accelerator section, final dump tank, and projectile decelerator. The light gas gun is capable of accelerating masses of 60 to 100 grams to speeds up to 1200 m/s. The muzzle of the gun has a perforated tube surrounded by an evacuated tank which serves to vent the helium driver gas.

The ram accelerator tube is 16 m long with a 38 mm bore. There are 144 instrumentation ports at 40 regularly spaced intervals along the accelerator tube. At 24 of these stations, there are four axial ports at right angles to each other. At the remaining stations, there are three ports separated by 120 degrees. This enables several different types of measurements to be taken at the same point along the tube. For every shot, these measurements include velocity, pressure distribution and luminosity. The 1 MHz digital acquisition system used to acquire the data has 32 channels. Multiplexing signals together allows up to 100 signals to be monitored during one shot.

The ram accelerator is designed to operate at propellant fill pressures up to 50 atm. Thin Mylar diaphragms contain the gas mixtures in the ram accelerator section as well as separate the sections of the tube filled with different propellant mixtures. The fuel, oxidizer, and diluent gases are metered and directed to the designated sections of the ram accelerator tube.

The end of the accelerator tube is connected to a 2.4 m long evacuated dump tank by a 0.76 m drift tube. The projectile flies freely through the dump tank where it can be photographed through a viewing port before it imbeds itself in tightly packed rug remnants in a 20 cm I.D. x 1 m long tube attached to the far end of the dump tank.

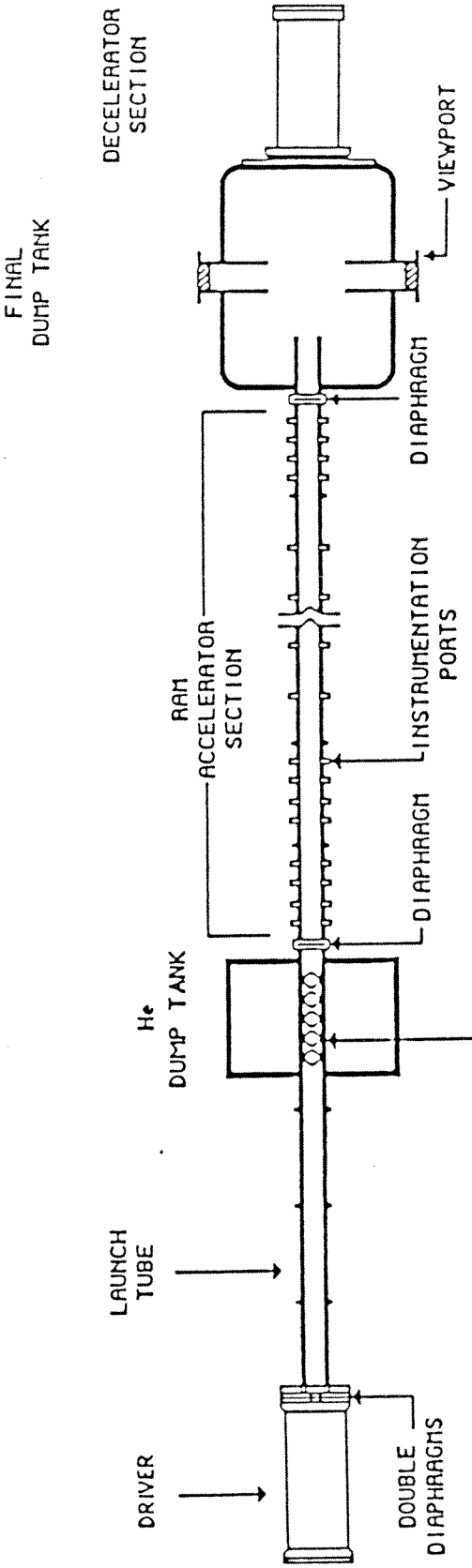

Fig. 2.1: Ram accelerator test facility.

The standard projectile geometry in use is illustrated in Fig 2.2. It is fabricated of aluminum in two pieces: the nose cone and the body with integral fins. The nose cone comes in two varieties: with a 10.0° or 12.5° cone angle. Both parts of the projectile are hollow and have an overall mass of 45 to 90 gm depending on internal detail. The projectile is sometimes nickel-coated for the purpose of providing a protective thermal shield. The benefit of this coating to ram accelerator propulsion has not yet been determined. The fins serve only to center the projectile in the tube. For a 38 mm bore tube, the maximum diameter of the projectile throat is 28.9 mm, in order to achieve a flow area ratio of 2.37 in the diffuser. Thin magnetic sheets are mounted in the nose-body joint, so that when the projectile passes by the electromagnetic transducers in the accelerator tube, the magnetic material induces signals used to determine the distance-time history and hence, velocity.

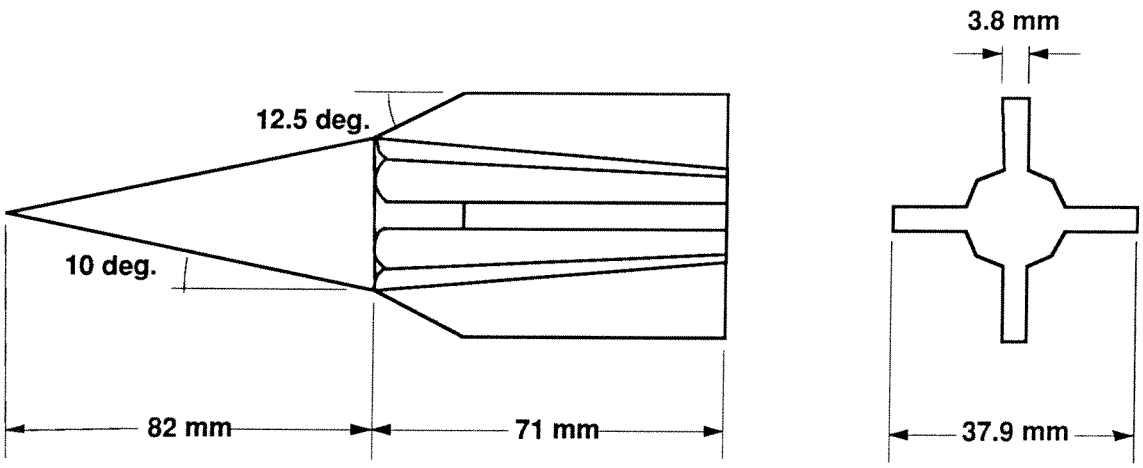

Fig. 2.2: Projectile geometry.

2.2 Instrumentation

In the current experiments, the first 6 m of the ram accelerator tube are configured into two stages. The length of tube containing the spectrometer probe was configured into the third stage. Sometimes a fourth stage followed.

Three types of information are monitored during every shot. The pressure transducers measure the pressure on the tube wall as the projectile passes with a response time on the order of one microsecond. The electromagnetic sensors are simply coils of

copper wire. As the projectile passes by the probe, the magnetic material at its throat induces a field through the coil. The pulse that is generated marks the passing of the projectile. The electromagnetic data from station to station provide time of flight information needed to calculate the projectile velocity. Photodetectors fed by fiber optic light guides are used to obtain luminosity profiles.

Figure 2.3 represents typical pressure, electromagnetic and luminosity signatures for an accelerating projectile in the thermally choked subsonic combustion mode at one station. In the pressure trace, there are several salient features that correspond to the conditions in a diffuser. The first pressure pulse is generated by the oblique shock system in the projectile's diffuser section. The increase in pressure after the oblique shock region is the normal shock which renders the flow subsonic. The pressure then decays because the heat addition chokes the flow.

The electromagnetic transducer sends a signal to the data acquisition system (DAS) when the magnetic material at the throat and rear of the projectile passes (magnetic material at the rear of the vehicle is sometimes omitted in order to reduce mass and increase acceleration). These signals are convenient reference points for analyzing the pressure and light data with respect to the projectile position.

The luminosity data reveal information about whether the nose tip is glowing, whether there is light on the body, and the extent of the combustion zone. Solid carbon particles (soot) are assumed to emit continuum radiation.

2.3 Combustion Zone Model and Theory

The combustion region is modeled as a flame stabilized on the blunt rear of the projectile, as shown in Fig. 2.4. The projectile base acts like a flame-holder. The recirculation zone is caused by the swirling gas flowing over the sharp edge at the rear of the projectile. Combustion occurs in the recirculation zone. The flame front is the thin shear layer between the free stream flow and the recirculation zone. Chemical equilibrium flow is assumed at full tube area.

The primary source of radiation is assumed to be blackbody from solid carbon (soot).[9] However, models for a soot-laden gas are difficult to formulate since experiments to measure particle size and distribution are very inaccurate. Many studies have been conducted on soot formation in methane and oxygen mixtures. Studies with stoichiometric mixtures of methane and oxygen have revealed that the actual free soot produced was lower than expected.[10] Additionally, experiments with methane and oxygen mixtures of $5CH_4 + 2O_2$ up to pressures of 100 atm have shown very little production of soot compared to

lower pressures.[10] The mixture in the third stage of the ram accelerator is currently $2.7CH_4 + 2O_2 + 13He$, and the pressures reached in the combustion region of the ram accelerator range from 300 to 500 atm. In explosion flames of stoichiometric methane and oxygen, water is one of the primary products. Mixtures similar to the ones used in the ram accelerator, were found to produce more CO and less water than stoichiometric mixtures.[10]

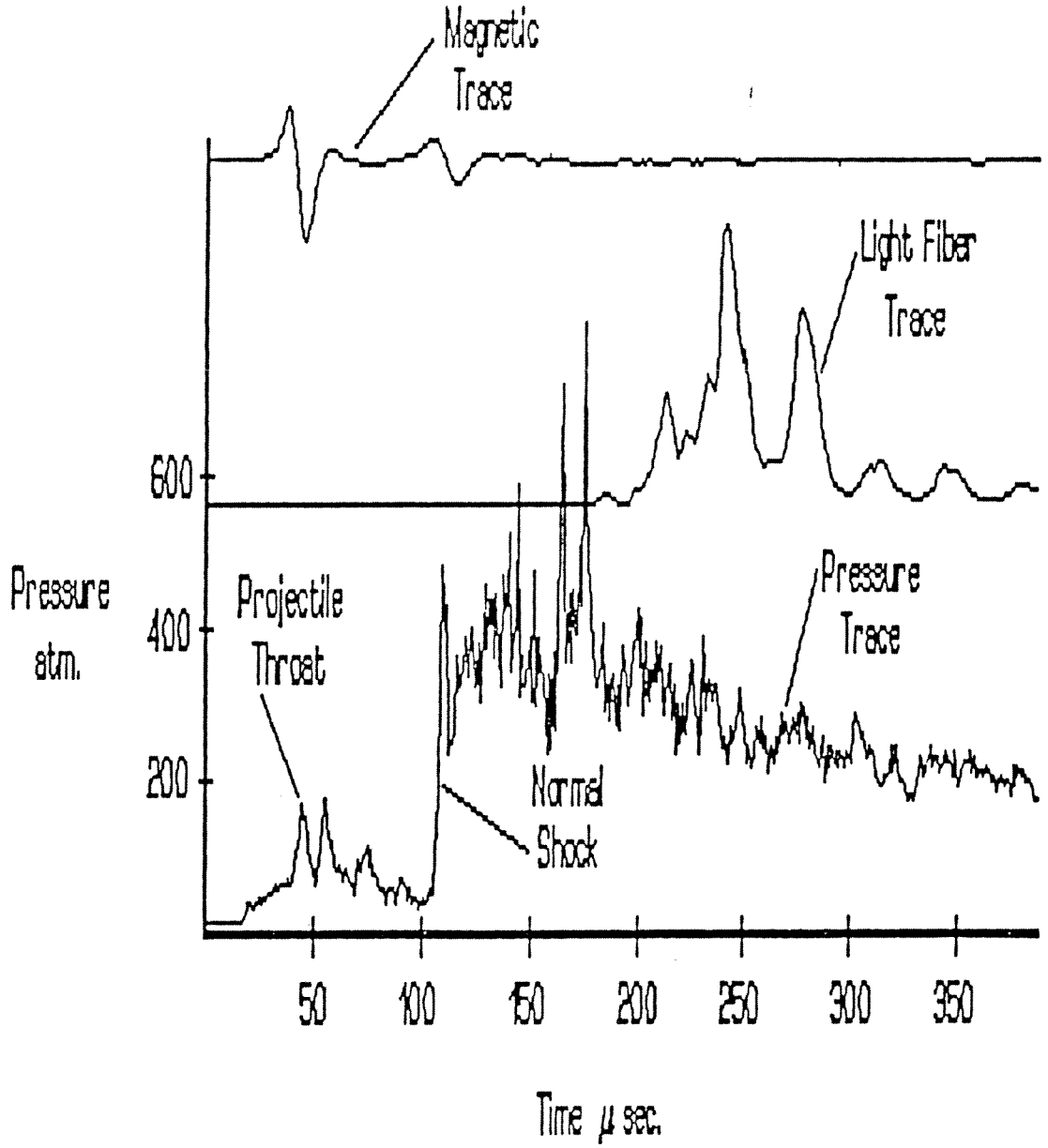

Fig. 2.3: Typical electromagnetic, pressure and fiber optic light guide signals.

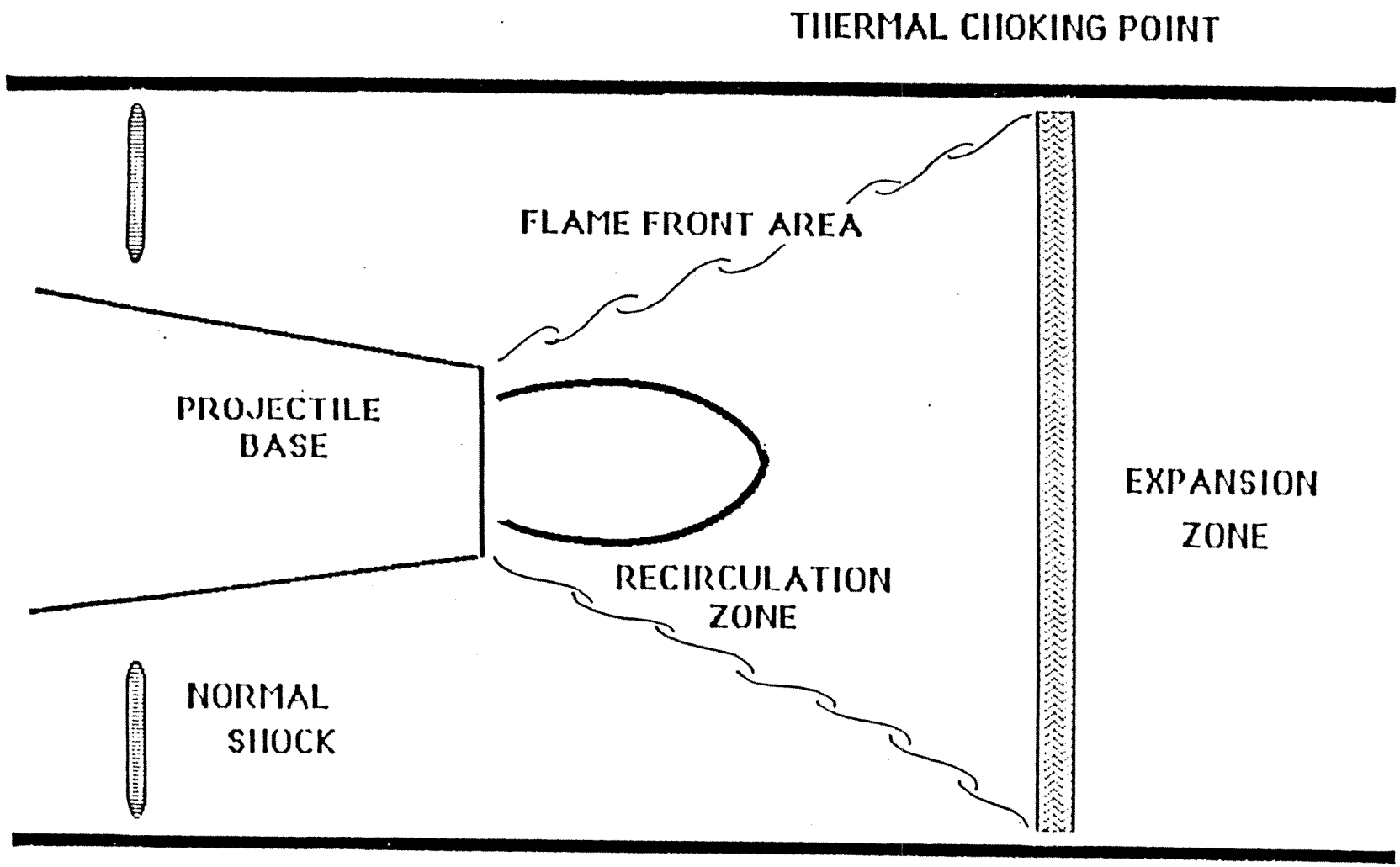

Fig. 2.4: Ram accelerator combustion zone.

Chapter 3

Experimental Apparatus

The light emitted during a single firing of the ram accelerator was collected by a fiber optic light guide flush with the inner wall of the tube. The fiber guided the light to the slit entrance of a spectrograph which was equipped with a charge coupled device (CCD) camera. The spectrograph has interchangeable and tiltable grating assemblies to allow a selection of wavelength coverage. The camera shutter is open for the duration of the shot (approximately four milliseconds). The light gathered by the camera is therefore time-integrated. The data are then read out, reduced and analyzed.

3.1 Optical Probe

The light from the ram accelerator was coupled to the spectrometer with a fiber optic light guide. A fiber with a pure silica core was chosen for its low attenuation over the spectral range of 400 to 1100 nm. The cladding was a hard polymer The length of the fiber was approximately 1 meter and was covered with a black sleeve to prevent damage. The fiber was mounted in a steel plug with epoxy, see Figure 3.1. A heat-cured epoxy, which was resistant to solvents, was chosen for the harsh environment it was exposed to in the ram accelerator tube. About 5 cm of the fiber buffer was mechanically removed to provide good adhesion. The inside of the plug was cleaned with a flux remover for the same purpose. After curing was complete, the end of the fiber was cleaved and polished to provide maximum light transmittance.

The fiber probes used to acquire broadband luminosity data are similar in design to Fig. 3.1. However, an acrylic fiber is used for practicality since the probes are taken out of the tube and cleaned after every shot. These fibers vary in length and are much more susceptible to damage. Information on the use of this probe in relation to the spectroscopic data will be developed in section 3.4. The fiber guide specifications for each probe are presented in Table 3.1:

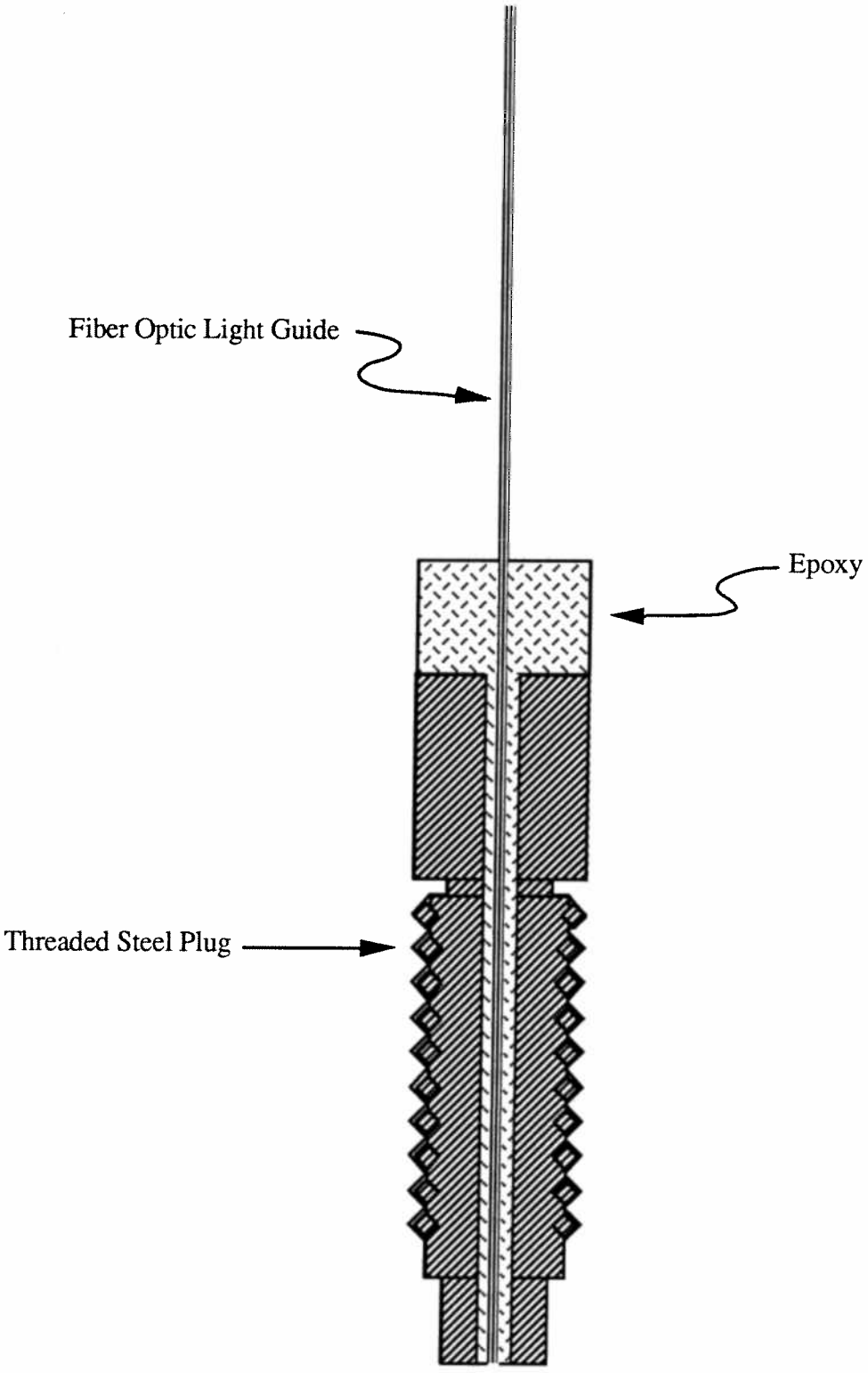

Fig. 3.1 Optical probe.

Table 1: Fiber Optic Light Guide Specifications.

Specifications	Spectrometer Probe	Luminosity Probe
Core Material	Pure silica	Polymethyl-methacrylate
Core Diameter	1.0 mm	1.0 mm
Outer Diameter	1.4 mm	2.2 mm
Maximum Attenuation	14 dB/km at 820 nm	160-250 dB/km at 660 nm
Numerical Aperture (NA)	0.37	0.47

3.2 Spectroscopic Apparatus

The Boller & Chivens Cassegrain Spectrograph was built for the University of Washington Astronomy Department by Perkin-Elmer in 1980. It was generously shared to help gather data for this thesis. The spectrograph was made to be used at the f/13.5 Cassegrain focus of a telescope and is essentially light-tight when mounted in this fashion. Figure 3.2 is a picture of the Cassegrain spectrograph in the ram accelerator facility. It is positioned approximately two-thirds (10 m) down the length of the ram accelerator test section. Figure 3.3 shows how the spectrograph was situated with respect to the ram accelerator tube. A schematic of the optical system is presented in Fig. 3.4. The available easy-to-use adjustments are slit width, collimator focus, and grating angle (Fig. 3.5). It is also equipped with a comparison He-Ne lamp. The focal length is 69 cm. The slit height is 2.5 cm. A slit width of 0.016 cm was selected in order to increase throughput. It was originally designed for plate photography, but has been adapted for use with a CCD camera by Patrick Waddell of the University of Washington Astronomy department.

The spectrograph was fitted with a grating blazed for 500 nm with a dispersion of 9.01 nm/mm (experimental) and was meant to be used in the first order blue. This grating has a ruled area 64 mm x 64 mm with 60 grooves/mm. An additional grating was mounted for this experiment. It had a blaze angle of 11°6' with 500 grooves/mm. These parameters

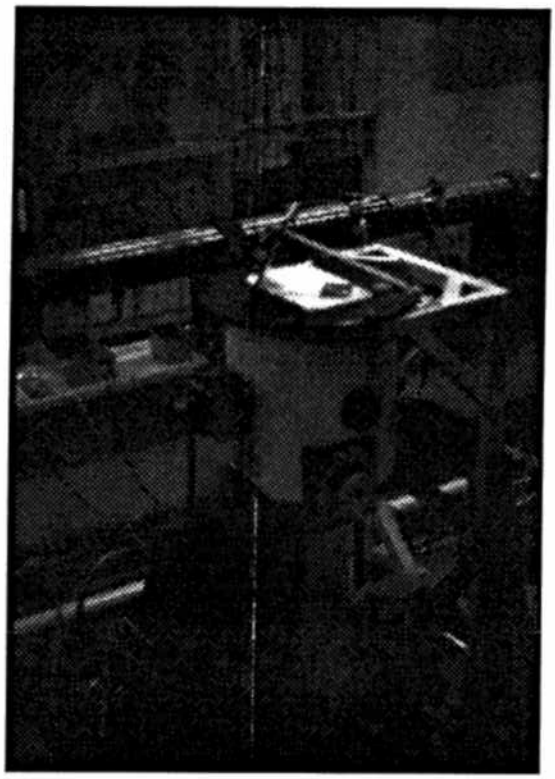

Figure 3.2 Cassegrain Spectrometer.

Figure 3.3 Spectrometer along side the ram accelerator tube.

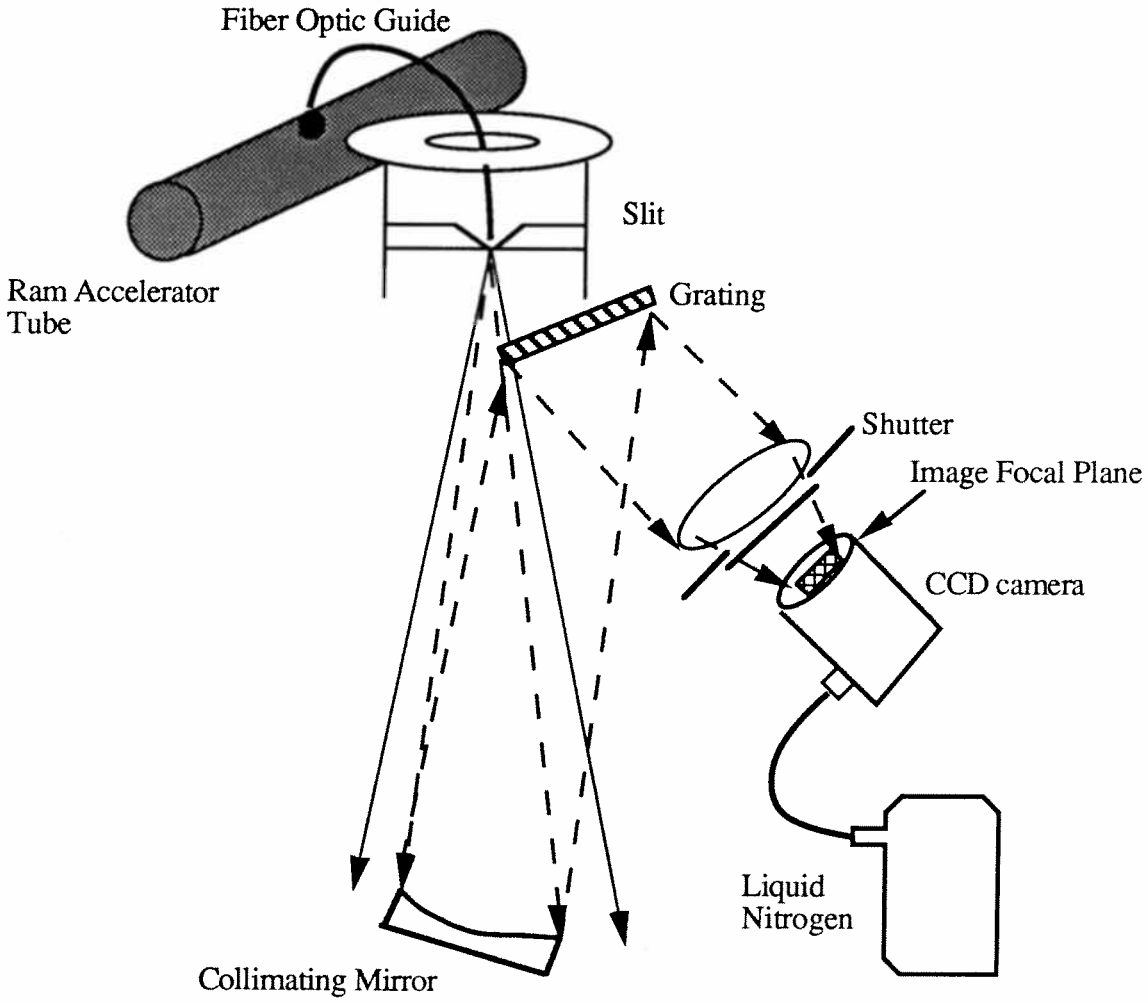

Figure 3.1: Optical system.

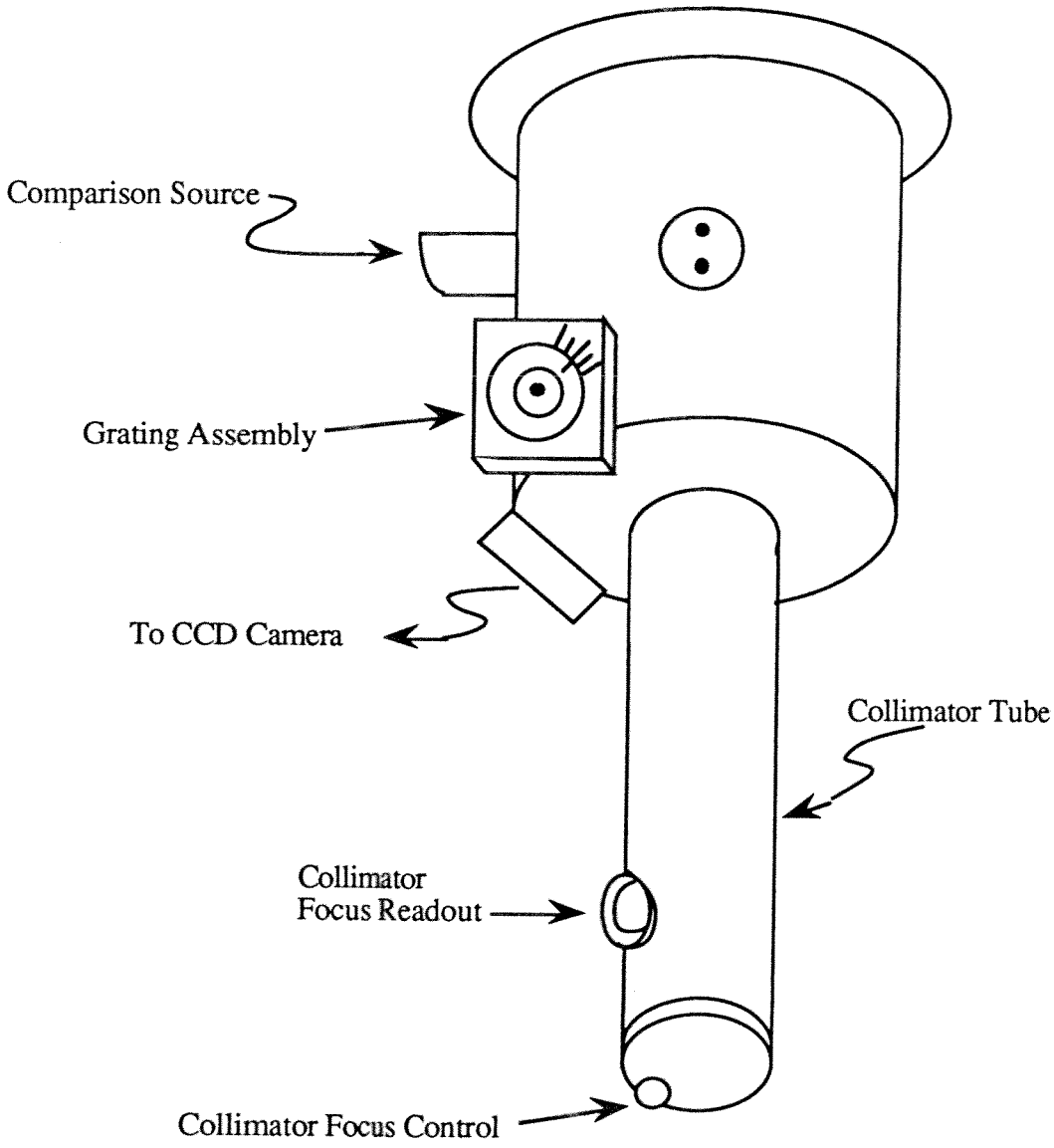

Figure 3.4: Spectrometer Configuration.

correspond to best efficiency at 770 nm. The dispersion was determined to be 10.7 nm/mm.

Coupling a fiber to a spectrometer is not the best way to analyze low-intensity emission. The efficiency of a fiber-fed spectrometer is very low. Fortunately, during the acceleration of a ram accelerator projectile, there is enough light radiated that a sufficient amount for spectroscopic puposes finds its way to the silicon detector or CCD array. The limiting factor of an optical system is called the "etendue".[11] Any light that does not fall within this limit is lost. The etendue of a spectrometer is the product of the entrance slit area and the accepting/transmitting solid angle. The solid angle, $\Omega = 2\phi/66^{o}$, where one steradian (sr) subtends approximately 66^{o} and the half angle, ϕ = arctan (a/2f) where a is the aperture and f is the focal length. Although the spectrometer is for an f/13.5 telescope, the collimator diameter is a little larger in order to catch all the light from the long slit. Even though this experiment does not use the whole slit height, the smaller effective focal ratio (f/#) matches the fiber numerical aperture (NA) better, thereby increasing throughput. Thus, for a 7.5 cm aperture, the focal ratio is effectively 9.2. For the Cassegrain spectrograph,

$$\text{etendue} = h \times w \times \Omega = (2.5)\,(0.016)\,(.0943) = 3.77 \times 10^{-3}\ \text{cm}^2\text{-sr}.$$

The etendue of the fiber is the product of the core area and the accepting/transmitting solid angle. For fibers, the half angle, δ = arcsin (NA). The etendue of the HCN fiber is 9.020×10^{-5} cm^2-sr.

The total useful light coupled to the spectrometer can be calculated using the area ratio of overlap:[11]

$$A_s / A_f = \left[2\,(f/\#) \tan (\arcsin NA) \right]^{-2}$$

The NA to focal ratio mismatch couples approximately 1.9% of the light. The percentage of the image that is not obstructed by the slit is given by the product of the fiber diameter and the width of the slit divided by the fiber core area (20.4%). Thus, the total useful light coupled to the spectrometer is (0.019 x 0.204) x 100 = 0.4%. Additionally, for each reflective surface, there is a 4% loss, so the light losses within the spectrometer due to the collimator and the grating further reduce the throughput to 0.36%. Using an all silica fiber optic light guide will increase the throughput by a factor of two. All silica fibers not only have a smaller NA but transmit a wider range of wavelengths (250 to 1200 nm).

3.3 Data Acquisition and Data Reduction

A sophisticated data acquistion system with a two-dimensional CCD array was used. The CCD camera was cryogenically cooled with liquid nitrogen to virtually eliminate dark current, or optical noise caused by thermal excitations. The CCD has excellent quantum efficiency for the range 300 to 1100 nm. The high resolution array is 1024 x 1024 with each pixel 15 μm on a side. Since the image height was approximately 300 microns, the image spanned 20 rows of the array. The rows were added on the chip, called binning. This increases the signal-to-noise ratio (S/N) by decreasing the amplifier noise added to the data during readout. The amplifier on readout induces approximately ten electrons of noise on the data. Surprisingly, in the first spectral data set taken in the near infrared (NIR) region, the CCD was saturated by light, so binnning was adjusted for data gathered in that spectral region thereafter. Figure 3.6 shows how the CCD is illuminated by the fiber guided radiation during a shot. Figure 3.7 shows the unreduced data of the peak row. The camera shutter was manually triggered before and after each shot, so the spectrum is time-integrated. The duration of radiation can be estimated from the luminosity data.

The data were calibrated by taking into account the background noise, spectral irradiance of the calibration lamp, and the throughput of the system. Figure 3.8 is the response function for the spectral region 650 to 790 nm with the grating with best efficiency at 770 nm. The response function of the system, which includes the fiber, spectrometer, and CCD, is obtained by directing the calibration lamp into the opposing port of the spectrometer probe. This data is preferably taken about two hours before the shot, however, shot schedules are often unpredictable and several days may elapse between the calibration readings and the shot data. Wavelength calibrations are also taken. Taking exposures with several different bandpass filters allows accurate determination of wavelength and grating dispersion. After the response function and wavelength calibrations are obtained, the ram accelerator tube is sealed, pressure-checked, and evacuated. About ten minutes before the shot, when the room is dark, a background reading or bias is taken. The bias contains all of the electrical offsets which is subtracted from all exposures when the data is reduced. Figure 3.9 is a typical bias. The response function of the system was calibrated using a quartz tungsten halogen (QTH) lamp. This source has a blackbody temperature of 3063 K. Figure 3.10 illustrates the suitability of this source for the wavelength region investigated. The flat field is obtained by dividing the response function by the normalized input function (Fig. 3.11). This flat field is then used to correct the shot

data resulting in Fig. 3.12. The y-axis of the data is in counts. Each count is equal to six electrons or photons detected at the CCD.

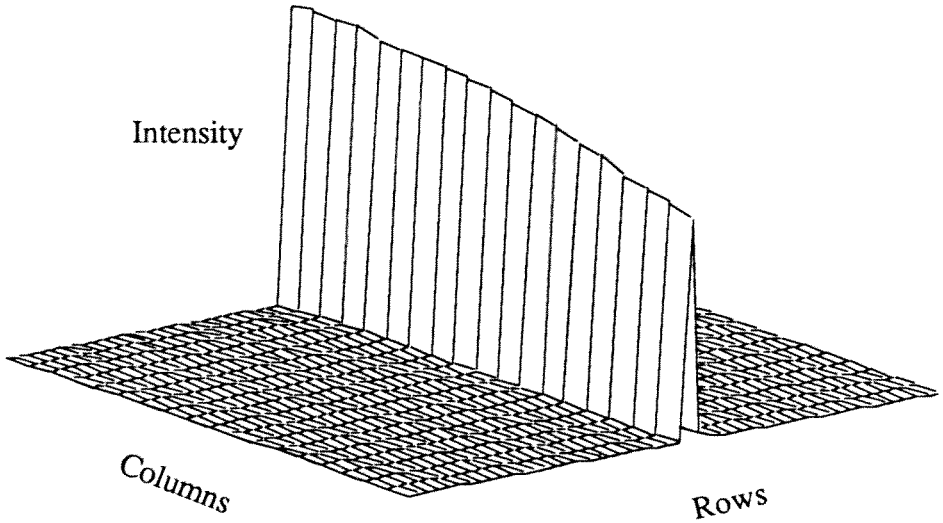

Fig. 3.6 CCD illumination during a shot.

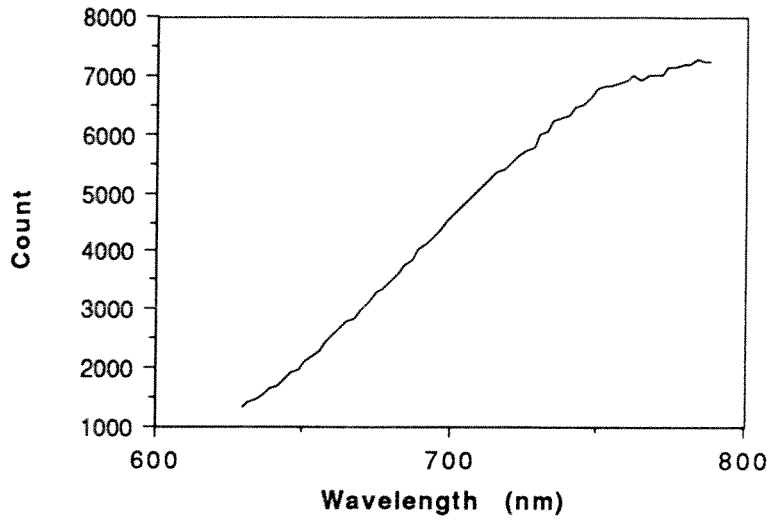

Fig. 3.7 Unreduced data set 3.

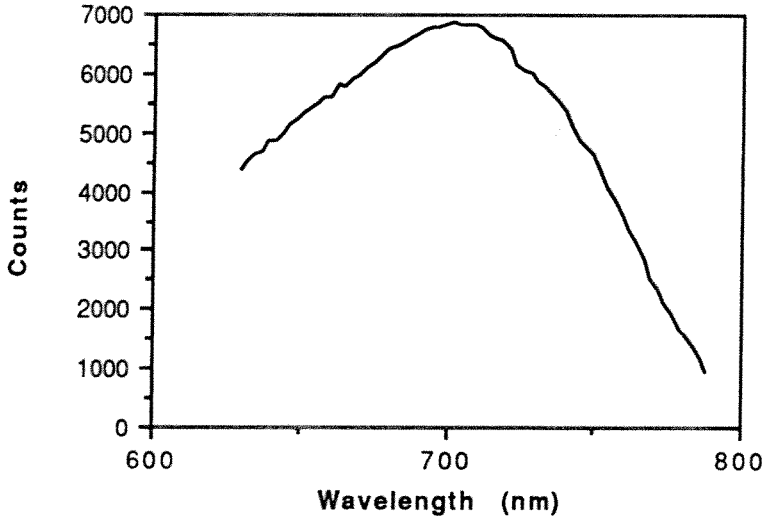

Fig. 3.8 Response function for data set 3.

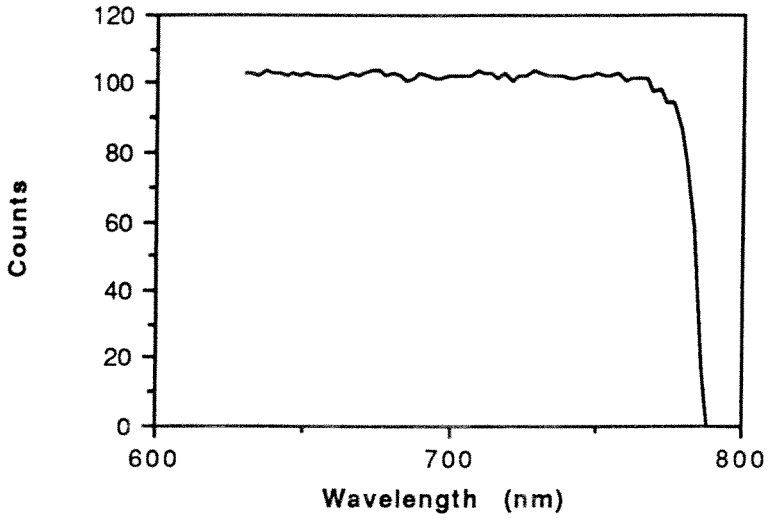

Fig. 3.9 Bias for data set 3.

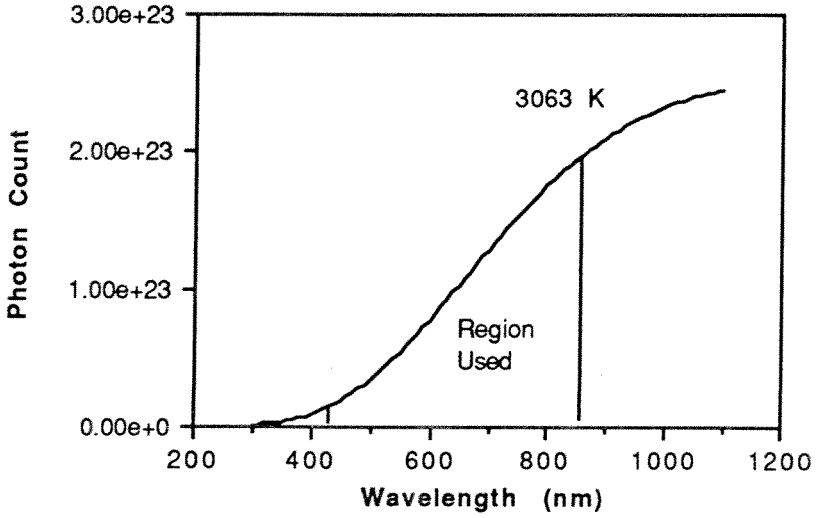

Fig. 3.10 Input function of quartz tungsten halogen lamp.

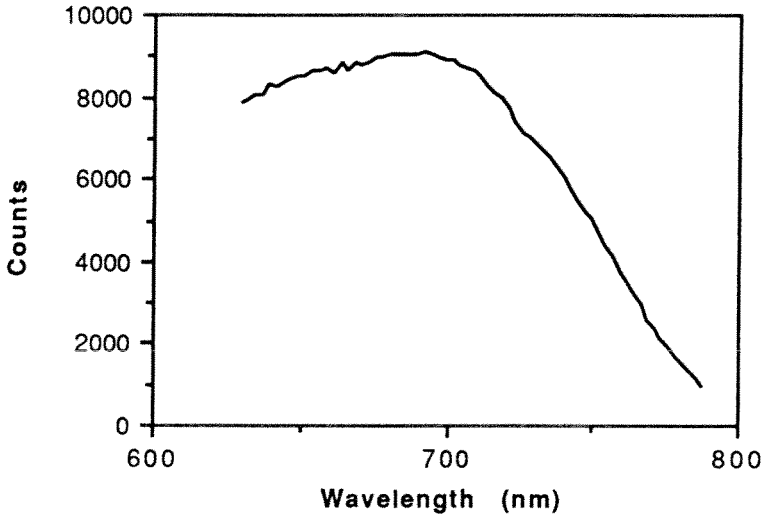

Fig. 3.11 Flat field for data set 3.

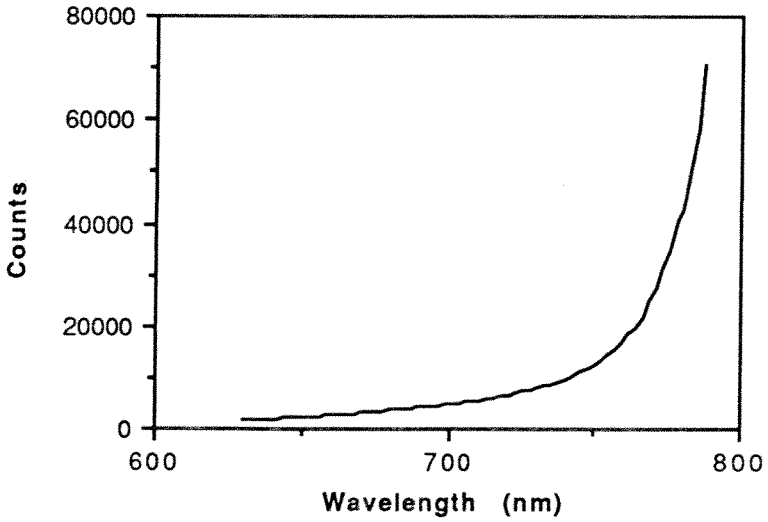

Fig. 3.12 Data set 3.

There is chromatic aberration in the optical system. As shown by Fig. 3.13, there is clearly some spatial distortion. This arises from the transverse magnification of the camera lens.[12] The center of the spectrum is on the axis of the camera lens and is therefore not distorted; the spectral lines off-axis are transversely magnified, and thus, distorted.

3.4 Luminosity Data

During a shot, light data are recorded from several stations along the tube. The luminosity emitted as the projectile and combustion gases pass by the probe is recorded. The light data correlated with the pressure distribution and projectile position and velocity provide complementary information about the processes in the tube. The luminosity data also aid the analysis of the spectral data. In addition to providing information of the radiation as a function of time, some of the light was filtered to obtain a rough analysis of how certain wavelength regions vary with time. With proper calibration of the photodetectors and improvements in the quality of fiber used, filtered light can be used to determine flame temperatures.

The system used to gather luminosity data consists of a fiber probe, photodetector, and data acquisition system (DAS). The specifications of the acrylic fiber optic are given in Table 1 in section 3.1. The optical fiber guides the radiation from the tube to a PIN photodiode. The photodiode has a photosensitive surface area of 5 mm^2. This allows up to 4 acrylic fibers to be multiplexed to one photodetector. The photodiode has a high responsivity in the visible to NIR regions. The signal is amplified and stored in the DAS along with the pressure and electromagnetic data.[9] Broad band filters were placed in front of some of the sensors during the spectroscopic investigations in order to obtain complementary data. Several broad band filters were used. Their spectral ranges were calibrated with a spectrophotometer. First, a broad background scan was taken and then each filter was placed between the slit and the calibration source. The blue filter at full width half maximum (FWHM) had a bandpass of 440 ± 6 to 500 ± 9 nm. The red filter at FWHM had a bandpass of 575 ± 12 to 725 ± 22 nm. The infrared filter was characterized with a bandpass of 735 ± 22 to 1000 nm.

Flame temperatures can be estimated using the two color temperature method.[13] The two color temperature method uses measurement of relative intensities over two wavelength regions. This can be done with spectral data or with two color filters. The assumptions about the variation of emissivity with wavelength are uncertain, so the result may not be very reliable. The spectral radiance of a blackbody is dependent on temperature

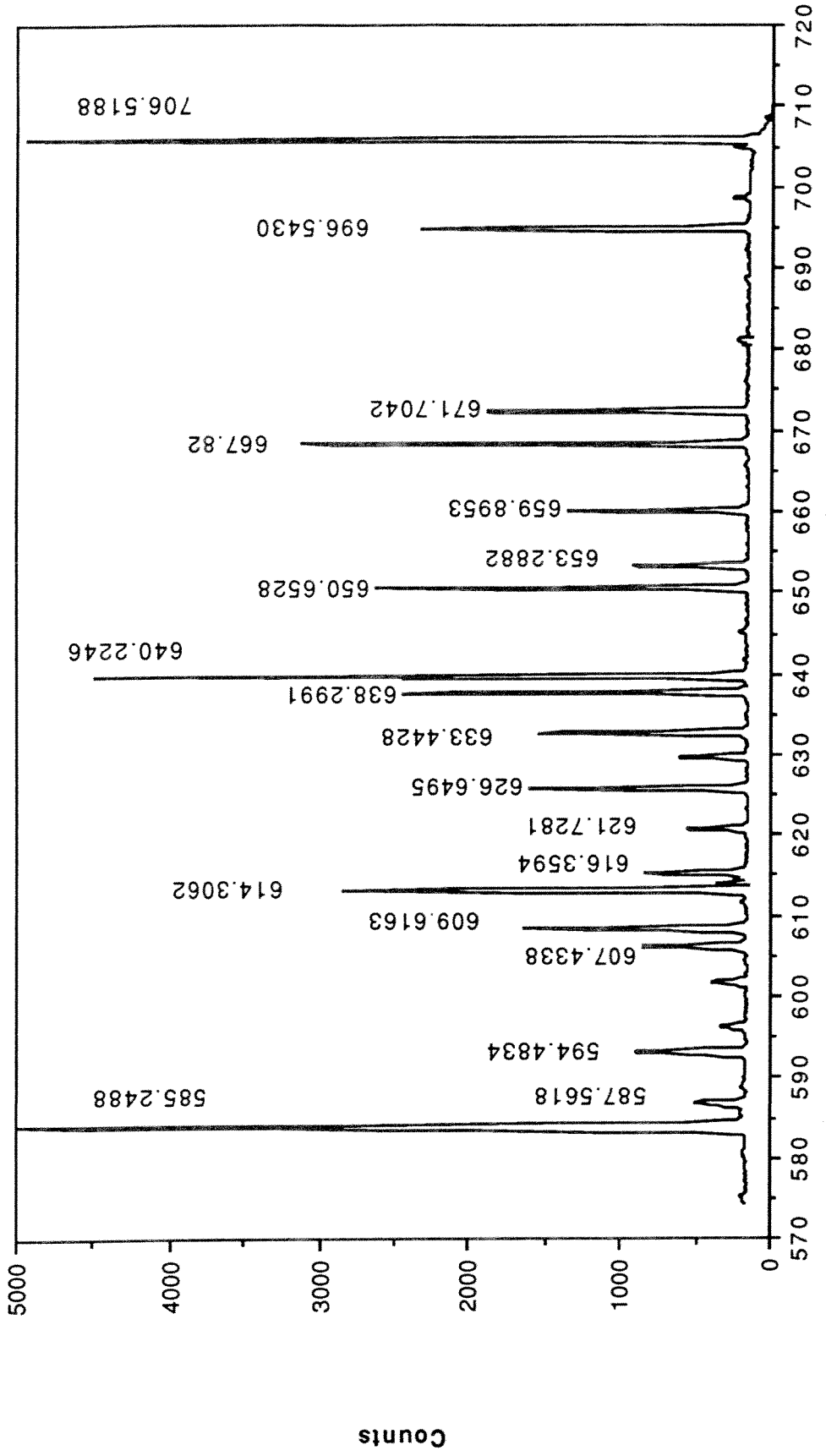

Fig. 3.13: Helium-neon spectrum.

only, but the spectral radiance of a gas is dependent on composition, pressure, and temperature.

There are several considerations to take into account before flame temperatures can be determined. First of all, the fiber optic cable itself is acrylic and has higher attenuation over the range of wavelengths studied. Second, several photodetectors are used to acquire the data, so they must be calibrated. There are also additional errors to consider in aligning the fibers with the sensors and the filters. Reflection of the light from the filters will decrease the throughput. Perhaps red and green filters would be more useful for flame temperatures because these spectral regions match the fibers' optical characteristics better.

Even without calculating flame temperatures these data are useful for overall light trends. The light data together with the pressure and projectile position data provide a qualitative view of the flow field. Luminosity data will accompany the spectral analysis in the following chapter.

Chapter 4

Results and Discussion

Spectra were obtained for eight shots. A summary of the propellant mixtures, fill pressures, velocities, Mach numbers and spectral regions investigated for each shot is presented in Table 2. The propellant mixtures for the third stage were very similar for the series of spectral investigations. The shot number refers to the number of the shot in the sequence of ram accelerator shots since operations began in October 1985. The data set numbers in the following text refer to the number of the shot in the sequence of the spectral experiments.

4.1 Data and Analysis

The processes that may contribute to radiation are combustion, shock heating, boundary layer combustion, ablation of aluminum, and shock-boundary layer interactions. The possible contaminants in the flow include aluminum particles, impurities in the aluminum, and lubricating oil used to clean the inside of the tube between shots.

As discussed earlier, two gratings were used. The first grating, blazed for 500 nm, was used for the first, second, and sixth data set. The second grating, blazed for 770 nm, was used for the other data. Binning by 20 was generally used (See section 3.3); however, data set 4 was binned by 7, and data sets 7 and 8 were binned by 3. The area on the CCD array on which photons impinge varies with binning, so the counts for data binned by lower numbers will be lower.

Table 2: Shot Summary

Data No.	Propellant Mixtures	Shot No.	Fill Pressure (atm)	Velocity (m/s)	Mach Number	Spectral Region (nm)
1	2.6CH4 + 2O2 + 13He	HS 779	43.2	2380	3.66	580-700
2	2.8CH4 + 2O2 + 14He	HS 781*	41.2	2290	3.50	580-700
3		HS 782*	41.8	2270	3.45	630-790
4		HS 783	35.0	2600 !	3.95	630-790
5	2.5CH4 + 2O2 + 13He	HS 786	39.1	3100 !!	4.75	710-860
6	2.7CH4 + 2O2 + 13He	HS 787	36.1	2280	3.50	420-540
7		HS 788	31.3	2300 !	3.54	710-860
8		HS 789	42.2	2270	3.50	710-860

* Nickel-coated projectiles

! Velocity of pressure wave after an unstart

!! Overdriven detonation wave

Data set 1 is presented in Fig. 4.1. It spans the wavelength range of 580 to 700 nm. The velocity at this station was 2380 m/s with a Mach number of 3.66. Figure 4.2 shows the luminosity data, pressure distribution, and throat position of the projectile at the same station.The y-axis is unlabeled since only the qualitative features of the traces are of relevance for this discussion. The duration of radiation was approximately 250 μs. Two stations farther down the tube (Fig. 4.3), the velocity increased to 2450 m/s, resulting in a Mach number of 3.76. Light on the nose of the projectile has developed. The throat position is marked by the electromagnetic signal. Thus, the second light feature is probably boundary layer heating on the body. The last feature is the light from the combustion. The time scale of these events is shorter than in Fig. 4.2. The combustion moved closer to the body. When the combustion region overtakes the projectile and merges with the pressure wave, an unstart ensues. The process no longer generates thrust on the projectile, but produces drag. The projectile unstarted in this shot 1.2 m farther down the tube. In Fig. 4.4, the combustion activity can be seen traveling with the pressure wave; this is a detonation wave.

Data set 2 is presented in Fig. 4.5. A nickel-coated projectile was fired in this shot, and the mixture was slightly different than for data set 1. The fill pressure and velocity were lower. The curve shape of data set 1 appears slightly broader than data set 2. The pressure, luminosity and EM traces associated with data set 2 are shown in Fig. 4.6. The luminosity data are much more defined than in Fig. 4.2. The light from the combustion region for the first shot seems diffuse. The nickel coating probably provided a protective surface to prevent ablation of the aluminum in the second shot.

Data set 3 (Fig. 4.7) was taken in the same mixture as data set 2 with a nickel-coated projectile as well. The second grating blazed for 770 nm was fitted for the spectrometer this shot. The wavelength region observed was 630 to 790 nm. The spectral curves from data sets 2 and 3 match very well. The luminosity data of data set 3 also match data set 2 and for that reason are not presented; the only variation is that a slight amount of nose light was detected at the spectrometric station in shot set 3. One might speculate the nickel coating on the projectile was not as well distributed as on the first nickel-coated projectile and has worn off. In fact, the second projectile did fail two stations earlier than the first.

Data set 4 was binned by 7 (Fig. 4.8). An attempt to trigger the CCD to acquire some time-dependent spectral features failed. The projectile propulsion also failed this shot before it reached the spectrometer probe and the resulting detonation wave damaged the fiber probe.

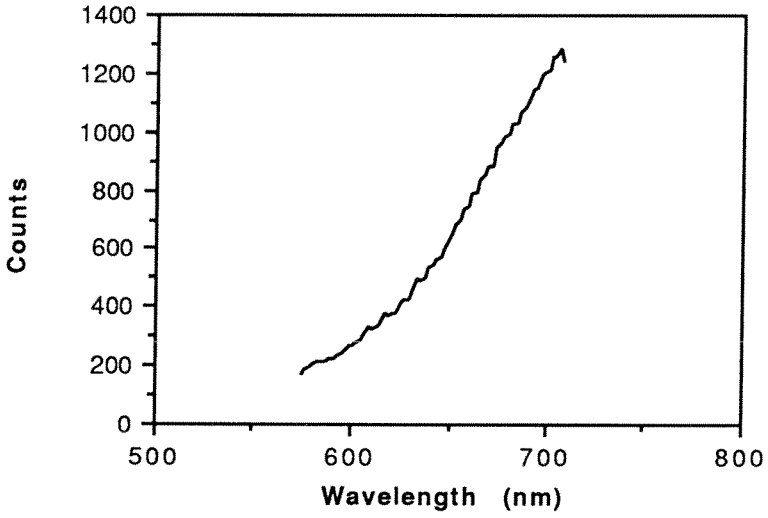

Fig. 4.1: Data set 1.

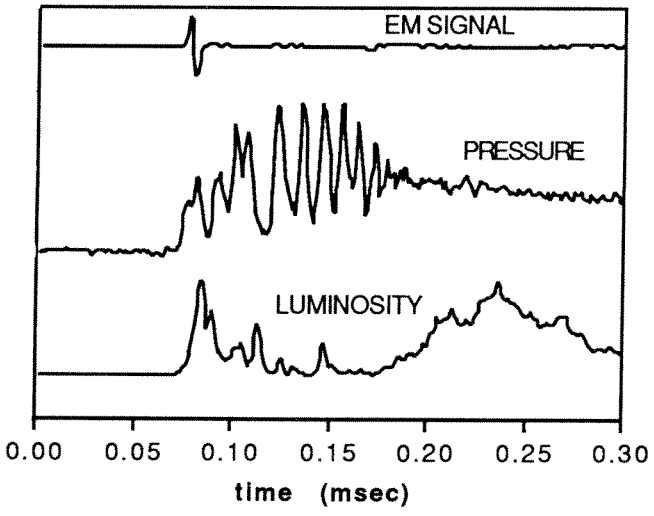

Fig. 4.2: Luminosity, pressure, and EM trace at the spectrometer station.

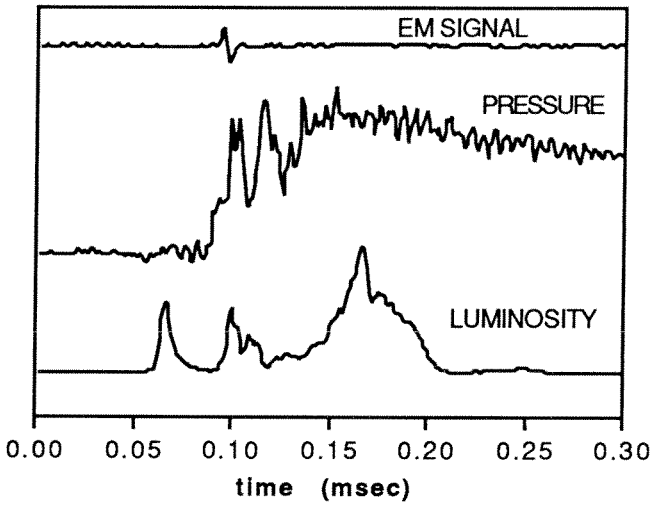

Fig. 4.3: Luminosity, pressure, and EM trace two stations farther down the tube.

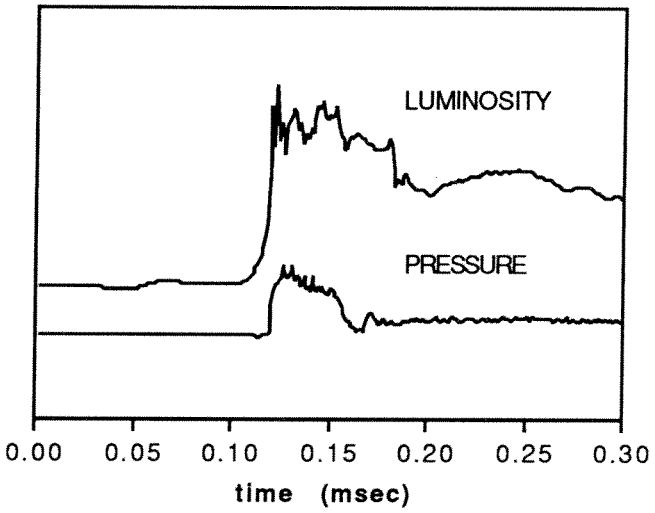

Fig. 4.4: Pressure and luminosity of a detonation Wave.

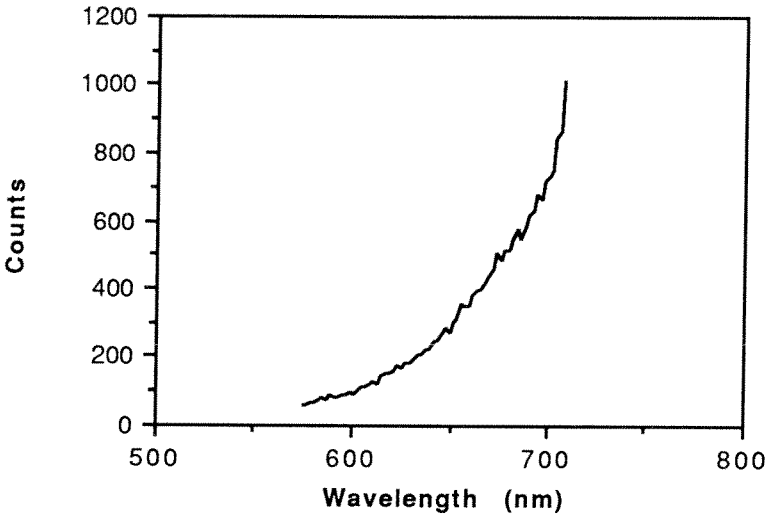

Fig. 4.5: Data set 2.

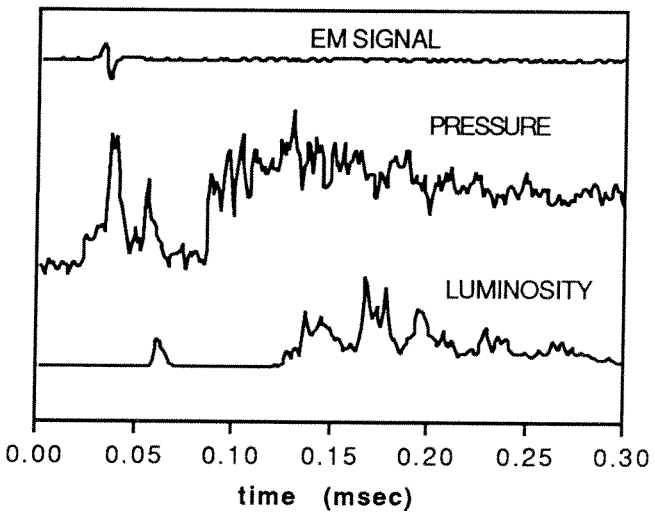

Fig. 4.6: Pressure, luminosity, and EM trace associated with data set 2.

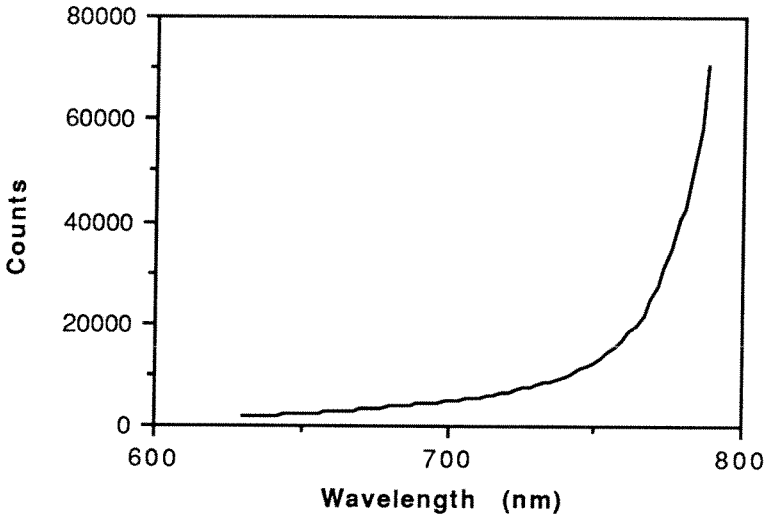

Fig. 4.7: Data set 3.

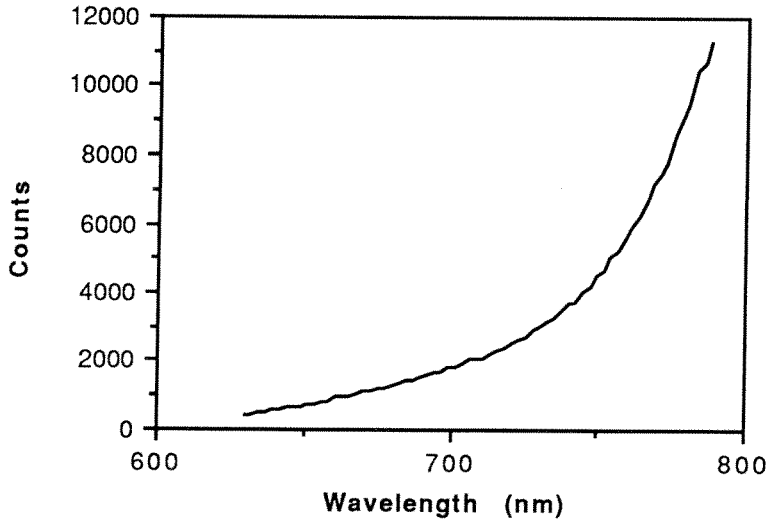

Fig. 4.8: Data set 4.

The unreduced data set 5 is presented in Fig. 4.9 because the CCD array was saturated. Only the few parts of the spectrum that were captured can be properly reduced. The projectile unstarted prior to reaching the spectrometer probe again, but this time the velocity of the detonation wave was faster than the C-J speed of the mixture. The wave velocity was approximately 3100 m/s. If the detonation occurs because combustion is too hot, the flow chokes at the throat and the projectile acts like a piston. In this way, the velocity of the wave can exceed the C-J detonation speed of the mixture; this is called an overdriven detonation wave. Although the CCD was saturated, O_2^+ absorption bands[14] were strong enough to be detected (Fig. 4.10). Detonation waves that do not travel at the C-J speed of the mixture have an unsteady structure. This could allow the absorption species to be between the radiation and the spectrometric probe. The concurrent luminosity data were taken with a blue filter in preparation for the following shot. This was a crude way to check if there were detectable light levels in the blue. These data did not contribute any information about the flow. However, the luminosity at nearby stations showed unusual duration. The radiation behind the shock wave lasts for about 250 μs and then the projectile passes followed by lingering combustion light.

Data #6 was very noisy. The wavelength region was 430 to 540 nm; the blue grating was used. Further investigations are necessary in this region. A suggestion for increasing the S/N is to use all silica fiber (instead of a silica core with a polymer cladding).

Figure 4.11 is spectral data set 7. The wavelength region is 690 to 845 nm and the data are binned by 3. These data are also from an unstarted condition. The velocity of the pressure wave was approximately 2300 m/s. The Chapman-Jouguet detonation velocity for this mixture was 2740 m/s. The peak of the radiation occurs around 835 nm. Near the peak radiation, a pressure-broadened absorption band is visible (See Fig. 4.12). An emission line for CO at 847.5 nm also appears to be present. No luminosity data were taken at the spectrometer station this time, but the luminosity data from two stations before the spectrometer station are given in Fig. 4.13.

Figure 4.14 is spectral data set 8. The projectile drove past the spectrometer probe at 2270 m/s. The wavelength where peak radiation occurs is very similar to that for data set 7. Both of these shots had the same propellant mixture, but the fill pressure of data set 8 was over 10 atm higher. An emission line near 847.5 nm where CO emits is again detected (Fig. 4.15). O_2 emits at 839.5 nm which appears to correspond to the feature labeled in Fig. 4.15. Additionally, the same pressure-broadened.absorption feature.seen in data set 7 manifests itself; to date the specie origin of this absorption has not been identified. The repeatability of these features lends credibility to their detection. The luminosity data at this

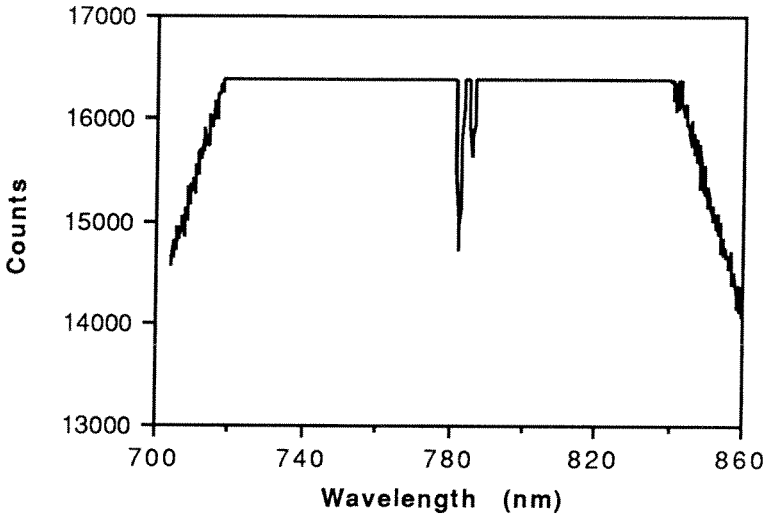

Fig. 4.9: Data set 5.

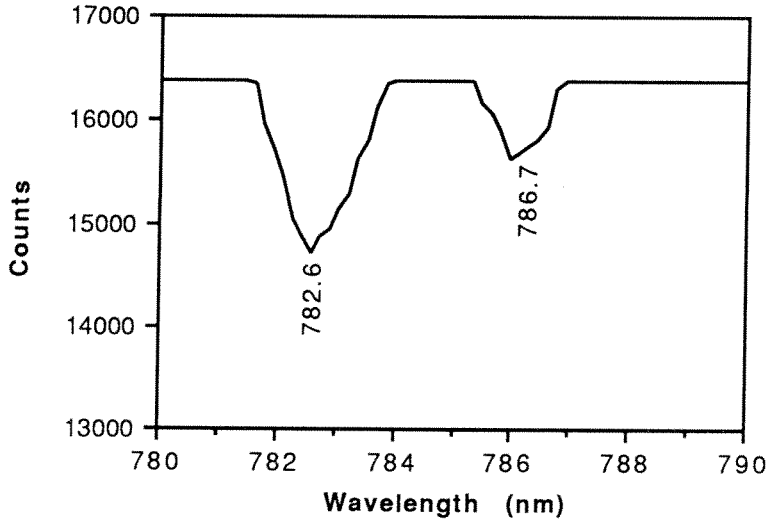

Fig. 4.10: O_2^+ absorption bands in the overdriven detonation wave spectrum.

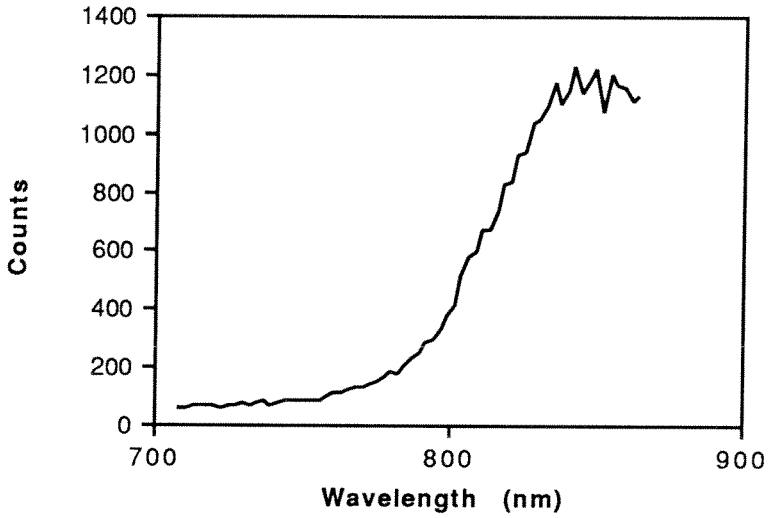

Fig. 4.11: Data set 7.

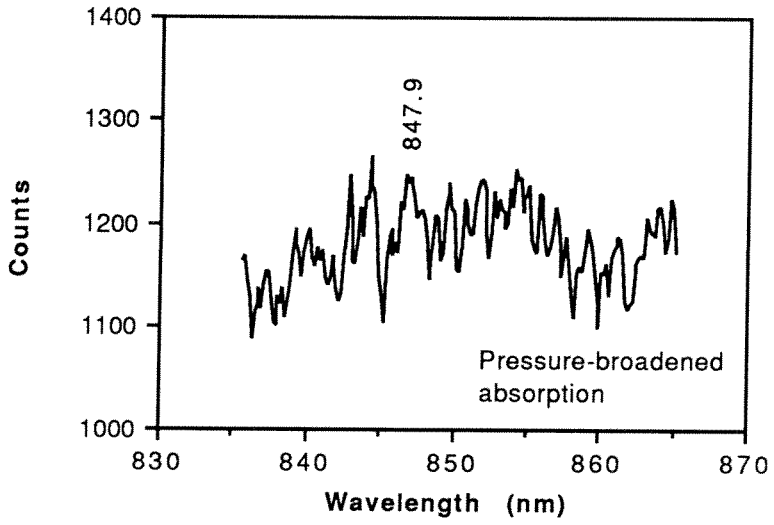

Fig. 4.12: Absorption and emission bands in data set 7.

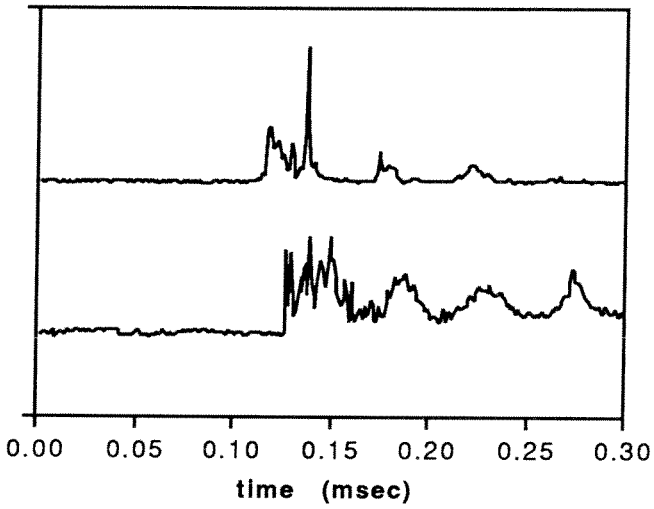

Fig. 4.13: Luminosity and pressure two stations before spectrometer station.

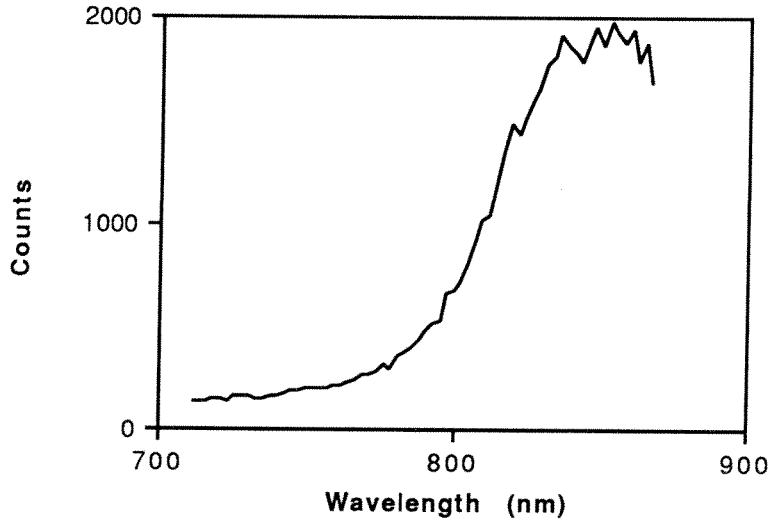

Fig. 4.14: Data set 8.

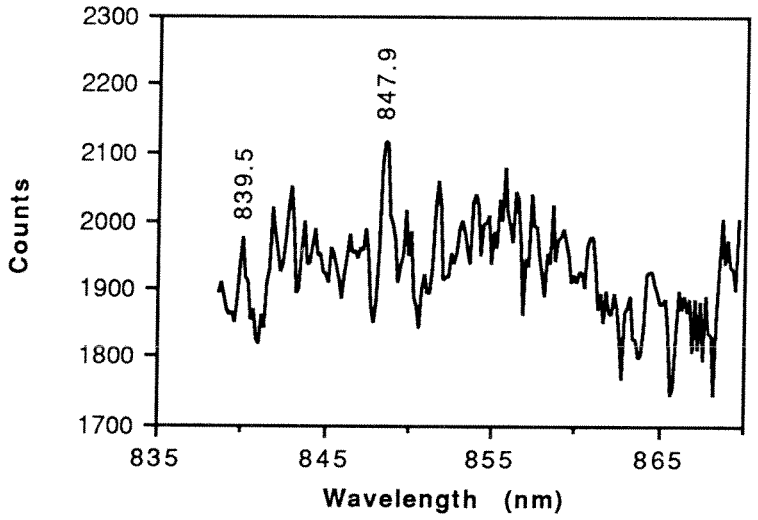

Fig. 4.15: Absorption and emission bands in data set 8.

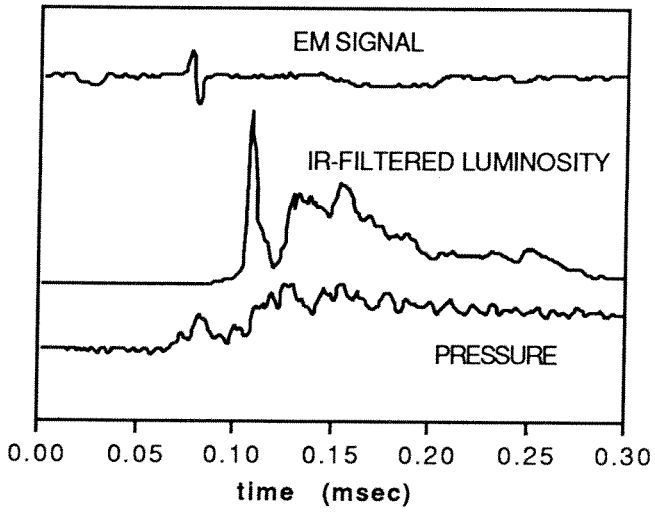

Fig. 4.16: Pressure, EM trace, and IR-filtered luminosity.

same station are shown in Fig. 4.16. The luminosity probe was newly constructed, so the fiber surface was very clean and unrecessed. The first light spike is associated with the normal shock on the body. The relative intensity of the normal shock light is much higher than the following combustion light suggesting that more species reacted in a shorter period of time, reminiscent of detonation wave light emission. Thus, more radiation was generated from shock heating than combustion itself.

Additional filtered light data were acquired from shot 780. These results are presented in the next section along with information on the reduction in transmission when the spectrometer probe is covered with soot.

4.2 Additional Results

Filtered light data from shot 780, immediately after the projectile unstarted, showed some interesting features. In Fig. 4.17, the IR-filtered light shows three pulses of radiation. Along with the first light pulse and pressure wave is an electromagnetic signal, probably from ionization. The drop in pressure after the first pulse (approximately 0.16 msec) is characteristic of the projectile position after an unstart. As the gases expand behind it, the gases cool down. The cooler gases emit very little light in the red, whereas, their radiation is still detectable in the IR. The IR pulses may be associated with the unsteady effects of a swirling or spinning detonation wave, but there are not any obvious perturbations in pressure to which the pulses of IR light correspond, as in Fig. 4.12. The different axial positions of these probes in the tube probably account for this. Asymmetry in luminosity data has been observed before[9], so there is probably pressure asymmetry as well. Solutions to the asymmetry of luminosity data that have been suggested include swirling of radiating carbon particles, optical density effects, unsteady effects, and variations in local temperature.[9]

To get an idea of how much intensity attenuation is caused by soot deposition on the face of the optical probe, a response function was recorded after the second data collection. As can be seen from Fig. 4.18, the reduction in transmission was approximately 20% at the midpoint of the data. This crudely estimates the effect of the soot deposition on the transmission of the fiber for this shot. The amount of soot generated depends on how fuel-richness of the propellant. The gas is assumed to be optically thick. In order for the effects of the soot-laden gas to be evaluated, an experiment to measure density and size distribution must be developed. This is beyond the scope of this thesis. Experiments of this kind would help model the flame-holder more accurately.

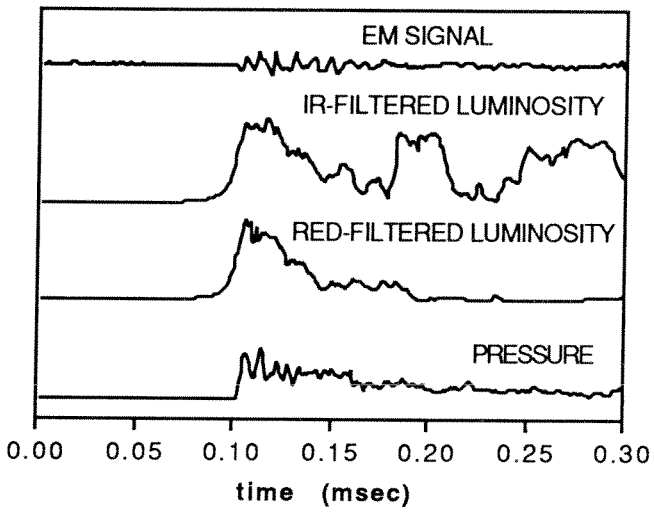

Fig. 4.17: Pressure, EM trace, red and IR-filtered luminosity immediately after the projectile unstarted.

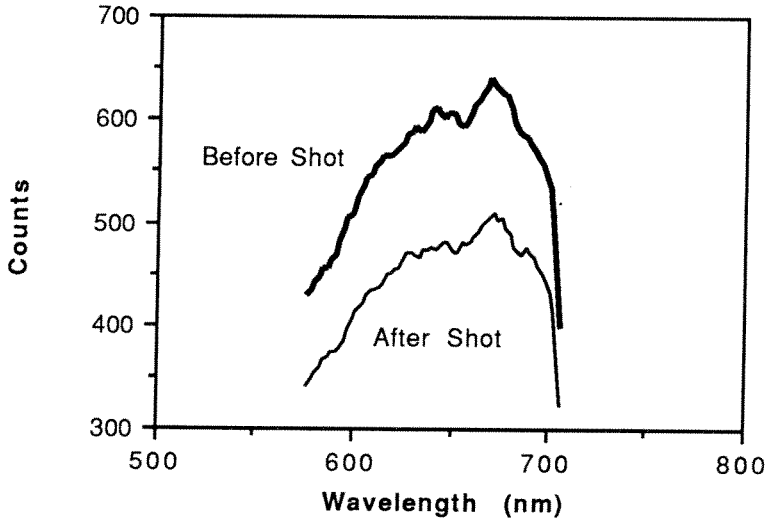

Fig. 4.18: Attenuation from soot deposition on the face of the optical probe.

Chapter 5

Conclusions

Preliminary spectral information was acquired for eight firings of the ram accelerator. Absorption bands as well as emission bands were detected in the NIR region. The detection of emission bands is promising for further sudies; time-dependent data may be able to separate the spectral characteristics of the shock-boundary layer interaction or shock-induced combustion from the combustion region.

In order to model the heat release, an accurate flame-holding model is needed. Experiments need to be developed for determining this. Also the ultraviolet wavelength region of 300 to 400 nm would be interesting to investigate since there should be strong emission from OH. Using an all-silica fiber will increase the signal-to-noise ratio and expand the wavelength region that can be studied. For a strong emission band, a photomultiplier tube with a selective filter for this wavelength could be used to obtain the concentration of that species as a function of time. Such information would be very helpful in modeling the heat release and verifying finite kinetics models.

Overall, optical measurements, and particularly spectrometric information, can be valuable in understanding the physics and chemistry of ram accelerator propulsion.

List of References

1. Hertzberg, A., Bruckner, A.P. and Bogdanoff, D.W., "Ram Accelerator: A New Chemical Method for Accelerating Projectiles to Ultrahigh Velocities," AIAA J., Vol. 26, pp. 195-203, 1988.

2. Bruckner, A.P., Bogdanoff, D.W., Knowlen,C. and Hertzberg, A., "Investigation of Gasdynamic Phenomena Associated with the Ram Accelerator Conept," AIAA Paper 87-1327, 1987.

3. Knowlen, C., Bruckner, A.P., Bogdanoff, D.W. and Hertzberg, A., "Performance Capabilities of the Ram Accelerator," AIAA Paper 87-2152, 1987.

4. Bruckner, A.P., Knowlen, C., Scott, K.A. and Hertzberg, A., "High Velocity Modes of the Thermally Choked Ram Accelerator," AIAA Paper 88-2925, 1988.

5. Bruckner, A.P., Knowlen, C., Scott, K.A., Hertzberg, A. and Bogdanoff, D.W., "Operational Characteristics of the Thermally Choked Ram Accelerator," to be published in Journal of Propulsion and Power.

6. Burnham, E.A., Kull, A.E., Knowlen, C., Bruckner, A.P., and Hertzberg, A., "Operation of the Ram Accelerator in the Transdetonative Velocity Regime," AIAA Paper 90-1985, 1990.

7. Kaloupis, Peter, "An Unsteady Total Variational Diminishing Axisymmetric Numerical Model for the Ram Accelerator Subsonic Combustion Thermal Choking Propulsion Mode," Masters Thesis, University of Washington, 1990.

8. Kull, Alan, "Preliminary Investigations of Superdetonative and Transdetonative Ram Accelerator Propulsion Modes," Masters Thesis, University of Washington, 1990.

9. Scott, K.A., "Experimental Investigation of Ram Accelerator Concept Using an Optical Probe," Masters Thesis, University of Washington, 1988.

10. Gaydon, A.G. and H.G. Wolfhard, Flames: Their Structure, Radiation, and Temperature, Chapman and Hall, New York, 1960.

11. Webb, Matthew J., "Practical Considerations When Using Fiber Optics with Spectrometers," Spectroscopy, Vol. 4, No. 6, 1989, pp. 26-34.

12. Hecht, Eugene and Alfred Zajac, Optics, Addison-Wesley Publishing Co., Reading, Massachusetts, 1979.

13. Siegel, Robert and John R. Howell, Thermal Radiation Heat Transfer, 2nd ed.,Hemisphere Publishing Corp., New York, 1981.

14. Herzberg, G., Molecular Spectra and Molecular Structure, v. 1, D. Van Nostrand Co., Inc., Princeton, N.J., 1959.